

Paediatric Phantom Dose Optimisation Using Digital Radiography with Variation of Exposure Parameters and Filtration whilst minimising Image Quality Impairment.

Lança, L.^{1,2}, Bowdler, M.W.³, Creedon, J.⁴, Dayer, V.⁵, Stensholt, N.⁶, Stuivenberg, V.H.⁷,
Pinhão, S.¹, Visser, M.B.⁷, Pires Jorge, J.A.⁵

¹ Escola Superior de Tecnologia da Saúde de Lisboa, Lisbon, PT

² Karolinska Institutet, Stockholm, SE

³ School of Health Sciences, University of Salford, Manchester, UK

⁴ University College Dublin, Dublin, IE

⁵ Haute École de Santé Vaud, University of Applied Sciences and Arts, Western Switzerland, Lausanne, CH

⁶ Oslo and Akershus University College of Applied Sciences, Oslo, NO

⁷ Department of Medical Imaging and Radiation Therapy, Hanze University of Applied Sciences, Groningen, NL

Abstract

Objective: To induce a reduction in dose, using a paediatric phantom, through the variation of exposure parameters and filtration, without adversely affecting image quality.

Methods: All images were acquired using a Kyoto Kagaku paediatric phantom and a Canon DR detector. The phantom was positioned supine for all projections: wrist (DP, lateral) and ribs (AP, oblique). Three dose protocols were established using different mAs values (high, medium and low) and copper (Cu) filtration was added to each protocol. DAP was used to calculate the ESD for each exposure.

Using ImageJ, CNR was calculated for the physical measurement of image quality. Image quality was assessed by fifteen observers (visual grading analysis (VGA)).

Results: The highest doses were recorded with the high dose protocol, ranging from 5.60-39.22 μ Gy for the wrist and 5.33-129.67 μ Gy for the ribs. When increasing the Cu filtration a decrease in ESD was observed. A difference of 0.1 in VGA score was noted between high and low dose protocols without the use of filtration, while a difference of 0.3 was noted when using filtration. As mAs increased, VGA scores increased. Fracture visibility was minimally affected by Cu filtration or projection variation.

Conclusion: The variation of exposure parameters in digital radiography can achieve a dose reduction without impairing image quality in bone fractures. Superior image quality can be achieved for DP and lateral wrist projections without Cu filtration. However, the addition of Cu filtration for the rib projections has almost no impact on overall image quality.

Introduction

Due to the detrimental effects of radiation, it is imperative that the dose received by the patient be as low as reasonably achievable (ALARA), whilst still obtaining images of a clinically acceptable standard (1). This is of particular importance when considering paediatric patients who, due to their additional life expectancy and increased tissue radio-sensitivity, are considerably more sensitive to the detrimental effects of ionising radiation (2). Although the radiation dose received for diagnostic purposes is low, it is pertinent that each exposure be

minimised due to the cumulative nature of radiation. This is because the cumulative dose received through multiple exposures can substantially increase the lifetime risk of certain cancers (3). Our work follows on from previous research (4–6) and further evaluates the plausibility of ascertaining decreased patient dose through modified exposure parameters, whilst assuring that the acquired images are clinically acceptable.

Several fundamental differences exist between conventional film-screen radiography and digital radiography. Hence, new protocols and strategies are required for effective optimisation in digital imaging (7). Various optimisation studies identify methods of dose reduction, by providing a systematic approach to recognising the factors that could be manipulated easily in a clinical setting (8). Our study assessed the impact of mAs and additional beam filtration on paediatric phantom dose and image quality. Copper (Cu) filtration is currently recommended for both adult and paediatric exposures, particularly if highly radiosensitive organs are directly exposed (9), and added filtration has been shown to reduce the overall effective dose for each individual paediatric exposure by up to 38% (8).

Paediatric digital radiography remains a challenge for many radiographers (10). The subsequent need for focused paediatric care is outlined by 'The Image Gently Campaign' (11), which reports a lack of both expertise and educational resources surrounding this area. This requirement is reinforced by The International Commission on Radiological Protection (ICRP), which identifies a need for both optimisation and consistency in digital paediatric imaging (12). Although a considerable proportion of recent research surrounds paediatric diagnostic imaging, Jones et. al highlights an absence of literature regarding optimisation in paediatric extremity imaging (6).

The question to be addressed through our study is as follows; using a paediatric phantom with multiple bone fractures, could the variation of exposure parameters and filtration in Digital Radiography achieve a reduction in dose without substantially affecting image quality?

The aim of our study was to induce a dose reduction for a paediatric phantom with bone fractures through the variation of exposure parameters and filtration without adversely affecting image quality.

Methods and Materials

Study Phantom

A Kyoto Kagaku 5-year-old (105cm/20kg) paediatric anthropomorphic phantom (PBU-70B) (Figure 1), was imaged. Fractures were present on the left side of the phantom (13)(14). Two regions were selected for this study, namely wrist and rib. Wrist fractures are one of the most commonly occurring fractures in paediatric patients and rib fractures have a considerable risk of misdiagnosis (15).

Imaging Systems and Positioning

All images were acquired using an Arcoma X-ray imaging system with DAP integration. The X-ray tube has the option to add 0.1, 0.2 or 0.3mm Cu filtration (16). All images were acquired on the same indirect Canon DR detector (CXDI-701C Wireless General Purpose) with a caesium iodide scintillator with a



Figure 1: Picture of the phantom used for this study (14)

detective quantum efficiency (DQE) of >70%. This detector has a pixel size of $125 \times 125 \mu\text{m}$ and an image matrix size of 2800×3408 pixels, with an effective imaging area of $35 \times 43 \text{cm}$. The resolution of the detector is 4.0lp/mm with 4096 gradations (17)(18). No anti-scatter grid was used during this study, as this would increase patient dose (19).

The phantom was imaged in the supine position for both antero-posterior (AP) and oblique rib projections. For the oblique projection, a radiolucent pad was

placed beneath the phantom, positioning the phantom at 20-degree obliquity. The collimated field remained constant at $15 \times 26 \text{cm}$, with a source-to-image-distance (SID) of 110cm. Dorso-palmar (DP) and lateral standard wrist projections were also acquired, with the collimated field fixed at $14.5 \times 8 \text{cm}$ and an SID of 110cm (20). A fine focal spot was used for both wrist projections, while a broad focal spot was used for both rib projections.

Protocol

A total of thirty-six images were acquired, nine for each projection. Three separate image acquisition dose protocols were used; low, medium and high. The high dose protocol employed standard exposure parameters, with tube potentials of 48kV and 52kV for the DP and lateral wrist projections, respectively. A tube intensity time product of 2mAs was applied for both DP and lateral wrist projections, when this was used (20). The high dose protocol employed 60kV and 0.63mAs for the AP rib projection and 68kV and 3.2mAs for the oblique rib projection (2). For each projection, the mAs was then lowered in two separate steps and low and medium protocols were constructed (Tables 1 and 2). For each protocol, the effect of Cu filtration was assessed using no filtration as well as 0.1mm and 0.2mm added Cu filtration.

Dose Measurement

Dose Area Product (DAP) values were derived using a calibrated integrated ionization chamber. DAP was then used to calculate the Entrance Skin Dose (ESD) for each exposure, using equation 1.

$$ESD = \left(\frac{DAB}{A} \right) * BSF \quad (\text{eq. 1})$$

The size of the collimated field is represented by A and the backscatter factor is represented by BSF. The

backscatter factor used throughout this study was 1.3, as recommended by Toivonen *et al* (21).

Image Quality

Contrast-to-noise ratio (CNR) was used to determine a physical measurement of image quality. CNR assesses the effect of changes in beam quality on image quality. ImageJ (22) was used to define regions of interest (ROIs) for CNR calculations. Four ROIs were placed on homogenous regions within each of the thirty-six total images, two on soft tissue and two on bone (Figure 2). For the two ROIs placed on soft tissue and the two placed on bone, a mean value was calculated to get more reliable measurements. CNR was then calculated using equation 2, where S_1 represents the mean pixel value within the ROIs placed on bone, and S_2 represents the mean pixel value within the ROIs placed on soft tissue. The σ_1 represents the standard deviation of bone (6)(23).

$$CNR = \frac{(S_1 - S_2)}{\sigma_1} \quad (\text{eq. 2})$$

Fifteen observers assessed visual image quality for each image through visual grading analysis (VGA). The observer group consisted of thirteen Radiography students of varying levels (years 1-4), as well as two experienced radiographers. ViewDEX was used to display the images, illustrate visual

Table 1: Wrist protocol with dose and image quality measurements

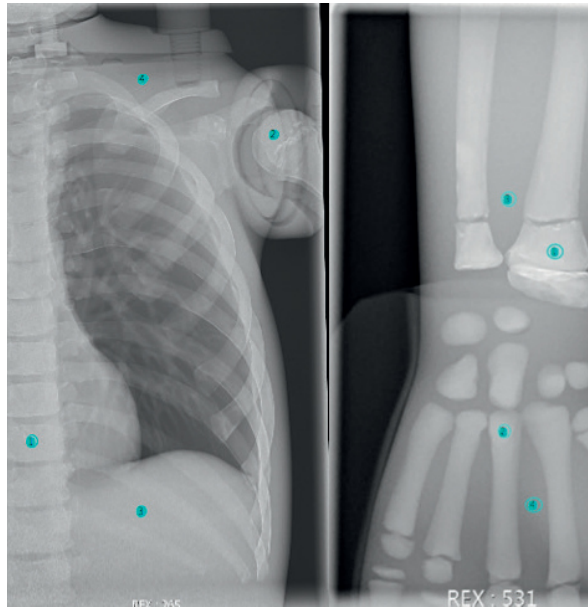
| Wrist | Projections | Kv | mAs | Cu Filter | CNR | DAP (mGy/cm ²) | ESD (μGy) | VGA _r |
|--------|--------------|----|-----|-----------|------|----------------------------|-----------|------------------|
| Low | Dorso-palmar | 48 | 0.5 | none | 10.4 | 0.7 | 7.84 | 3.5 |
| | | | | 0,1mm | 5.5 | 0.3 | 3.36 | 2.5 |
| | | | | 0,2mm | 3.7 | 0.1 | 1.12 | 1.7 |
| | Lateral | 52 | | none | 13.3 | 0.9 | 10.09 | 3.1 |
| | | | | 0,1mm | 10 | 0.3 | 3.36 | 2.4 |
| | | | | 0,2mm | 6.9 | 0.2 | 2.24 | 1.8 |
| Medium | Dorso-palmar | 48 | 1 | none | 14.4 | 1.4 | 15.69 | 3.8 |
| | | | | 0,1mm | 8.3 | 0.5 | 5.6 | 3.1 |
| | | | | 0,2mm | 5.5 | 0.3 | 3.36 | 2.3 |
| | Lateral | 52 | | none | 15.1 | 1.7 | 19.05 | 3.8 |
| | | | | 0,1mm | 12 | 0.8 | 8.97 | 3.1 |
| | | | | 0,2mm | 10 | 0.3 | 3.36 | 2.4 |
| High | Dorso-palmar | 48 | 2 | none | 16.2 | 2.8 | 31.38 | 4.2 |
| | | | | 0,1mm | 11.4 | 1.1 | 12.33 | 3.3 |
| | | | | 0,2mm | 7.6 | 0.5 | 5.6 | 3.1 |
| | Lateral | 52 | | none | 16.3 | 3.5 | 39.22 | 4.1 |
| | | | | 0,1mm | 15.6 | 1.4 | 15.69 | 3.7 |
| | | | | 0,2mm | 11.4 | 0.8 | 8.97 | 3.1 |

Table 2: Ribs protocol with dose and image quality measurements

| Ribs | Projections | Kv | mAs | Cu Filter | CNR | DAP (mGy/cm ²) | ESD (μGy) | VGA _r | |
|--------|-------------|----|------|-----------|-------|----------------------------|-----------|------------------|-----|
| Low | AP | 60 | 0.4 | none | 4.7 | 3.9 | 13 | 3 | |
| | | | | 0,1mm | 3.9 | 1.8 | 6 | 2.6 | |
| | | | | 0,2mm | 2.9 | 1 | 3.33 | 2.2 | |
| | Oblique | 68 | | 2 | none | 2.3 | 24.6 | 82 | 3.5 |
| | | | | | 0,1mm | 1.8 | 12.5 | 41.67 | 3.4 |
| | | | | | 0,2mm | 1.5 | 7.7 | 25.67 | 3.1 |
| Medium | AP | 60 | 0.5 | | none | 5 | 4.9 | 16.33 | 3.1 |
| | | | | | 0,1mm | 4.1 | 2.3 | 7.67 | 2.9 |
| | | | | | 0,2mm | 3.5 | 1.3 | 4.33 | 2.5 |
| | Oblique | 68 | | 2.5 | none | 2.2 | 30.6 | 102 | 3.7 |
| | | | | | 0,1mm | 1.9 | 15.6 | 52 | 3.4 |
| | | | | | 0,2mm | 1.5 | 9.7 | 32.33 | 3.1 |
| High | AP | 60 | 0.63 | | none | 5.9 | 6.1 | 20.33 | 3.5 |
| | | | | | 0,1mm | 4.6 | 2.8 | 9.33 | 2.8 |
| | | | | | 0,2mm | 3.6 | 1.6 | 5.33 | 2.7 |
| | Oblique | 68 | | 3.2 | none | 2.3 | 38.9 | 129.67 | 3.7 |
| | | | | | 0,1mm | 1.8 | 19.9 | 66.33 | 3.3 |
| | | | | | 0,2mm | 1.6 | 12.4 | 41.33 | 3.4 |



Figure 2: ROIs for the wrist DP and rib AP views, with ROI 1 and 2 on bone and ROI 3 and 4 on soft tissue



scoring criteria and also collect observer scores (24). Prior to image-viewing, the observers were trained in the visual assessment task in order to maximise validity and reliability. The observers could pan and zoom, but the use of windowing was prohibited. They were made aware of the fracture location prior to rating the images. The observers first scored the eighteen wrist images, followed by a short break, before scoring the eighteen rib images. All images were randomized and observers were blinded to acquisition conditions and exposure factor information. A five-point Likert scale was used to assess five criteria: overall image quality,

contrast, sharpness, noise and fracture visibility. With this scale, a score of 1 indicates Poor, while that of 5 indicates Excellent. Numerical scales as such are often used to simplify information and to improve inter-observer agreement (24). Ambient lighting conditions in the observation room remained constant throughout the image-viewing process at less than 10 lux (25)(26). The monitor used for observer analysis was also fixed throughout the study, with an area of 32.4x43.2cm.

Images were displayed on a 21.3-inch Monochrome LCD monitor MS25i2 (ML21025), manufactured by



Totoku™ (27), calibrated to the DICOM greyscale standard (28). All observer information was anonymised. The total VGA (VGA_T) was calculated using equation 3.

$$VGA_T = \frac{\sum_{O,I} S_c}{N_I N_O} \quad (\text{eq.3})$$

In equation 3, S_c represents each criterion score given by the observers, O represents the observer and I represents the image. N_I represents the total number of images and N_O is the total number of observers (29). A separate VGA score was calculated using the three primary visual image quality parameters; contrast, sharpness and noise (VGA_{CSN}) (30). This score was calculated by adding the observer scores from these three criteria and generating a mean value. The VGA_{CSN} was then correlated with fracture visibility for each projection.

Statistics

Descriptive statistics were used to analyse the data. This data was imported to Statistical Package for the Social Sciences (SPSS). Mean VGA, CNR and R^2 correlations were calculated using Excel. A very high correlation is noted between 0.90 and 1, while a high correlation is between 0.70 and 0.90. A moderate correlation is seen between 0.50 and 0.70 (31). An independent samples Kruskal-Wallis non-parametric

test was used to analyse statistically significant differences at 95% confidence level between the 15 observers regarding VGA.

Ethics

As this study involved the use of an anthropomorphic phantom and no human subjects, ethical review was not necessary. All observers gave their informed consent prior to this study, through their participation in the OPTIMAX 2017 summer school.

Results

Dose Protocols

Table 1 highlights the protocols for wrist with dose and image quality measures: kV, mAs, ESD and VGAT. As expected, dose measurements and CNR decreased with added filtration. The average reduction for all three filters was identical for DP and lateral wrist projections, at 76%. The most substantial reduction in image quality occurred with 0.2mm added Cu filtration. Overall, the addition of filtration reduced dose for all projections, however this results in an overall reduction in image quality. VGAT is lower with the addition of filtration.

Table 2 demonstrates the relationship between dose measurements (DAP and ESD), CNR, and VGA_T for each of the three dose protocols for both rib projections. The primary focus of this table is on AP and oblique rib projections and again, both dose

and CNR values decreased with added filtration. For the AP rib projection, with no added filtration, there was a 36% dose decrease from high to low dose protocols, with an equal decrease between both high and medium, and medium and low dose protocols. However, the VGA_T differed by merely 0.1 between high and low dose protocols with no added filtration. When 0.1mm Cu filtration was added, there was a comparable dose decrease of 36% between high and low dose protocols, with an 18% decrease between high and medium dose protocols, and a 22% decrease between medium and low dose protocols. However, the VGA_T differed by just 0.3 between high and low dose protocols with 0.1mm added filtration. With 0.2mm added Cu filtration, there was a similar dose decrease of 38% from high to low dose protocols, with a 19% decrease between high and medium protocols and a 23% decrease between medium and low dose protocols. Again, the

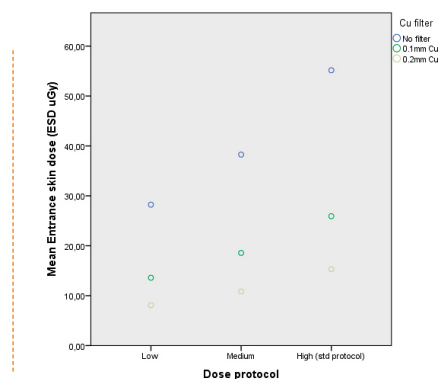
VGA_T differed by just 0.3 between high and low dose protocols, with 0.2mm added filtration.

For the oblique rib projection, with no added filtration, there was a 37% dose decrease from high to low dose protocols, with a reduction of just 0.2 in VGA_T . When 0.1mm Cu filtration was added, there was a similar 37% reduction in dose, with an increase of 0.1 in VGA_T . With 0.2mm added filtration, there was a dose decrease of 38% and a reduction of just 0.3 in VGA_T . A dose variation of 20-22% was found between high and medium, and medium and low dose protocols, for all three filtration settings for all three dose protocols.

Dose Measurements

Figure 3 demonstrates the combined mean ESD for the high, medium and low dose protocols for wrist and ribs. As expected, the highest doses were recorded using the high dose protocol. The dose

Figure 3: Mean ESD for each protocol and Cu filtration level



levels ranged from 8.09-28.23 μ Gy, from 10.85-38.27 μ Gy and from 15.31-55.15 μ Gy for the low, medium and high dose protocols, respectively. There was an overall decrease in ESD with added Cu filtration, as seen in Figure 3. There was a 51.8% reduction in ESD when 0.1mm Cu filtration was added, with the low dose protocol. The entrance surface dose was reduced by 47.7% and by 53.0% for the medium and high dose protocols, respectively. A greater dose reduction was achieved with 0.2mm added Cu filtration, at 71.4%, 71.6% and 72.2% for the low, medium and high dose protocols.

Contrast-Noise-Ratio Measurements

Figure 4 displays the mean CNR for each projection and for each of the three dose protocols. A wide range is seen in CNR values for both wrist projections, with that of the DP wrist varying between 3.7 and 16.2

and that of the lateral wrist varying between 6.9 and 16.3. The difference between CNR values for both rib projections, however, is much less varied, ranging between 2.9 and 5.9 for the AP projection, and 1.5 and 2.3 for the oblique projection. As expected, the CNR for all exposures decreased with increased filtration, for all three dose protocols.

Quality of Phantom Images

As seen in Tables 3 and 4, VGA_{CSN} scores increase as mAs increases. However, with added filtration, a notable reduction is seen in image quality scores for all projections. This reduction is marked in the DP wrist projection, with a reduction of 2.07 for the low dose protocol, 1.53 for the medium dose protocol, and 1.27 for the high dose protocol. A similar reduction in image quality is seen in the lateral wrist projection, with a decrease of 1.2 for the low dose

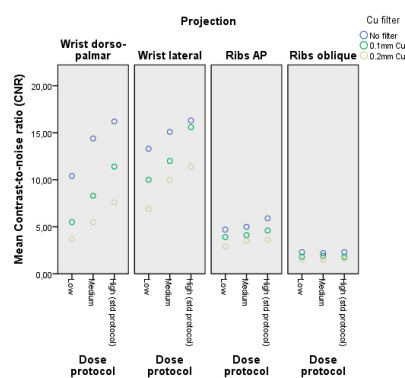


Figure 4: Mean CNR for each protocol and Cu filtration level

Table 3: Wrist image quality visual grading scores and CNR

| Ribs | Projection | Kv | mAs | Cu Filter | Overall Image quality score (SD) | VGA _{CNR} (SD) | Fracture visibility (SD) | CNR |
|--------|------------|----|------|-----------|----------------------------------|-------------------------|--------------------------|-----|
| Low | AP | 60 | 0.4 | none | 3.07(0.64) | 2.98(0.31) | 3.20(1.15) | 4.7 |
| | | | | 0.1mm | 2.73(0.76) | 2.60(0.27) | 2.67(0.96) | 3.9 |
| | | | | 0.2mm | 2.20(0.92) | 2.09(0.17) | 2.47(1.13) | 2.9 |
| | Oblique | 68 | 2 | none | 3.53(0.64) | 3.71(0.37) | 2.73(1.16) | 2.3 |
| | | | | 0.1mm | 3.47(0.74) | 3.58(0.42) | 2.60(1.03) | 1.8 |
| | | | | 0.2mm | 3.20(1.00) | 3.24(0.29) | 2.60(1.13) | 1.5 |
| Medium | AP | 60 | 0.5 | none | 3.13(0.59) | 3.07(0.24) | 3.20(0.52) | 5 |
| | | | | 0.1mm | 3.00(0.74) | 2.87(0.00) | 3.07(0.70) | 4.1 |
| | | | | 0.2mm | 2.53(0.65) | 2.42(0.14) | 2.47(0.94) | 3.5 |
| | Oblique | 68 | 2.5 | none | 3.87(0.74) | 3.93(0.12) | 3.07(0.74) | 2.2 |
| | | | | 0.1mm | 3.47(0.74) | 3.53(0.18) | 2.93(0.83) | 1.9 |
| | | | | 0.2mm | 3.00(0.64) | 3.27(0.04) | 2.47(1.12) | 1.5 |
| High | AP | 60 | 0.63 | none | 3.60(0.63) | 3.51(0.04) | 3.40(0.99) | 5.9 |
| | | | | 0.1mm | 2.93(0.70) | 2.78(0.21) | 2.93(1.03) | 4.6 |
| | | | | 0.2mm | 2.87(0.74) | 2.51(0.33) | 2.93(0.80) | 3.6 |
| | Oblique | 68 | 3.2 | none | 3.67(0.82) | 3.93(0.24) | 3.13(1.30) | 2.3 |
| | | | | 0.1mm | 3.20(1.15) | 3.60(0.64) | 2.67(1.29) | 1.8 |
| | | | | 0.2mm | 3.33(0.98) | 3.64(0.43) | 2.80(1.21) | 1.6 |

Table 4: Ribs image quality visual grading scores and CNR

| Wrist | Projection | kV | mAs | Cu Filter | Overall Image quality score (SD) | VGA _{CNR} (SD) | Fracture visibility (SD) | CNR |
|--------|--------------|----|-----|-----------|----------------------------------|-------------------------|--------------------------|------|
| Low | Dorso-palmar | 48 | 0.5 | none | 3.47(0.92) | 3.29(0.10) | 4.20(0.77) | 10.4 |
| | | | | 0.1mm | 2.20(0.76) | 2.27(0.07) | 3.47(1.19) | 5.5 |
| | | | | 0.2mm | 1.40(0.63) | 1.33(0.12) | 2.93(1.39) | 3.7 |
| | Lateral | 52 | | none | 2.80(0.68) | 3.02(0.21) | 3.60(1.12) | 13.3 |
| | | | | 0.1mm | 2.20(0.94) | 2.27(0.18) | 2.93(1.22) | 10 |
| | | | | 0.2mm | 1.60(0.74) | 1.67(0.18) | 2.60(1.35) | 6.9 |
| Medium | Dorso-palmar | 48 | 1 | none | 3.73(0.80) | 3.69(0.27) | 4.27(1.08) | 14.4 |
| | | | | 0.1mm | 3.13(0.70) | 2.76(0.41) | 4.07(0.82) | 8.3 |
| | | | | 0.2mm | 2.20(0.77) | 1.96(0.28) | 3.33(0.92) | 5.5 |
| | Lateral | 52 | | none | 3.73(0.83) | 3.71(0.27) | 4.20(1.03) | 15.1 |
| | | | | 0.1mm | 2.93(0.83) | 3.00(0.32) | 3.60(1.06) | 12 |
| | | | | 0.2mm | 2.33(0.77) | 2.22(0.38) | 3.20(1.18) | 10 |
| High | Dorso-palmar | 48 | 2 | none | 4.27(0.80) | 4.13(0.17) | 4.57(0.88) | 16.2 |
| | | | | 0.1mm | 3.40(0.74) | 3.00(0.10) | 4.27(0.96) | 11.4 |
| | | | | 0.2mm | 3.00(0.77) | 2.78(0.14) | 4.20(1.18) | 7.6 |
| | Lateral | 52 | | none | 4.13(0.59) | 4.07(0.17) | 4.13(0.77) | 16.3 |
| | | | | 0.1mm | 3.60(0.70) | 3.6(0.20) | 3.87(0.99) | 15.6 |
| | | | | 0.2mm | 3.13(0.90) | 2.91(0.27) | 3.60(1.08) | 11.4 |

protocol, 1.4 for the medium dose protocol, and 1 for the high dose protocol. A decrease is also noted in overall image quality for both rib projections, however this is far less apparent, with a reduction of 0.87 for the low dose protocol, 0.6 for the medium dose protocol and 0.73 for the high dose protocol for the AP rib projection. For the oblique rib projection, there was a reduction of 0.33 for the low dose protocol, 0.87 for the medium dose protocol, and 0.34 for the high dose protocol.

Fracture visibility was minimally affected by beam filtration and projection variation. For the DP wrist, a difference of just 0.37 was noted between low and high dose protocols, with no added filtration. Similarly, a difference of just 0.53 occurred between low and high dose protocols for the lateral wrist, with no added filtration. A negligible difference of 0.2 was noted in fracture visibility for the AP rib projection between high and low dose protocols, and a difference of 0.4 was noted in the oblique rib projection. VGA_{CSN} scores follow a similar pattern to

overall image quality scores, with decreasing values as Cu filtration is added. For all projections, using all protocols, fracture visibility also decreased as Cu filtration was added. It is clear from these tables that overall fracture visibility was higher in the wrist than in the ribs.

Visual and Physical Image Quality Measurements

For each of the four projections, the fracture visibility scores were correlated with both physical (CNR) and visual measurements (VGA_{CSN}) (See Table 5). A strong correlation was found between CNR and fracture visibility for both DP and lateral wrist projections. CNR and fracture visibility for the AP rib projection also shows a strong correlation. Regarding the oblique rib projection, a moderate correlation was found between CNR and fracture visibility. Similar findings can be seen in the relationship between VGA_{CSN} and fracture visibility, with the strongest correlations occurring in the DP wrist, lateral wrist and AP rib projections. The weakest correlation was found in the oblique rib projection (See Table 5).

| Projection | CNR vs Fracture Visibility | VGA_{CSN} vs Fracture Visibility |
|------------|----------------------------|------------------------------------|
| | | |
| | | |
| | | |

The distribution of mean ratings was the same across all fifteen observers, showing no significant statistical difference in VGA_T score between observers ($p=0,450$). A strong correlation was found between the physical measurement of CNR and the visual analysis of each image. This correlation was weaker for the oblique rib view than for the remaining three projections.

Discussion

This study aimed to reduce radiation dose without adversely affecting image quality, using a paediatric phantom with multiple bone fractures. This involved the variation of exposure parameters and beam filtration settings. The low dose images produced in this study have shown that reducing the dose has minimal impact on fracture visibility. However, the CNR values vary widely between dose protocols and anatomical regions. Similar findings were also reported in other studies (6). The CNR values reported for the rib projections are markedly lower than those of the wrist projections. This notable decrease was reflected in comments from the observers, reporting difficulty in fracture visualisation. However, this difficulty could also be due to phantom positioning and the superimposition of anatomical structures, particularly in the oblique view.

The results of this study show a strong correlation between visual and physical measurements for each projection, reinforcing our findings. This strong correlation poses the question: Are both physical and visual measurements needed for image quality analysis? Similarly, overall image quality scores were similar to VGA_{CSN} values, suggesting that overall image quality may be sufficient for predicting fracture visibility and image quality. Similar outcomes were found in other studies (30). The standard deviation for inter observer assessment is low, meaning that observers agreed with one another about each criterion.

The most striking result found in this study was the effect of Cu filtration on both dose and image quality, with added filtration consistently reducing patient dose, at the cost of image quality. The values for ESD and DAP found in this study mirror those found in published research (15)-(20). Physical measurements were calculated for each of the thirty-six images using the CNR, a common method of image quality measurement, whereas visual measurements were obtained as fifteen observers rated the images. However, this study used predominantly radiography students as observers and further research is suggested with the aid of experienced radiologists and radiographers to allow a comparison with clinical practice.

The primary focus of this study was on wrist and rib fractures as wrist fractures are among the most common paediatric fractures (32), and rib fractures are associated with high rates of misdiagnosis (15). In patients between the ages of two and four, the largest proportion of limb fractures occur in the upper limb (76.0%), the most common of which are in the distal humerus (22.0%) and the distal radius (21.3%) (32). Similarly, in children between the ages of five and eleven, the most common fracture location is the distal radius (40.3%) (32). In cases of abuse, however, many fractures occur in the ribs, the most acute of which are frequently missed on initial imaging (15). This constitutes an important topic for further research in the clinical context, regarding the optimization of exposure in the paediatric population.

The results of this research are valid in the context of this study and this constitutes the major limitation as cannot be valid in the clinical context. Although it has been well documented that DR detectors allow the production of good quality images at low exposures due to their high associated DQE, further research is suggested in clinical practice, using real paediatric patients. This will help to better determine the technical factor modifications needed to achieve safe radiographic practice at low exposure levels, while maintaining image quality. Secondly, the phantom used may not have been entirely anthropomorphic, with various different materials and their associated

X-ray absorption properties. However, the use of a phantom allowed multiple repeated exposures, with maintained absorption properties.

Furthermore, different hospitals may use different positioning methods, detectors and parameters for paediatric patients, when compared to those used throughout this study. However, this does not mean that the parameters used in this study cannot be adapted and applied in clinical practice.

Conclusion


Using digital radiography, the variation of exposure parameters can achieve a reduction in dose, without impairing diagnostic image quality or fracture visibility. Superior image quality can be achieved for DP and lateral wrist projections at higher doses, without the use of Cu filtration. However, the addition of Cu filtration for the rib projections can reduce phantom dose with almost no impact on overall image quality. Overall, the addition of filtration reduced dose for all projections.

Acknowledgments

The authors would like to thank Oslo and Akershus University College of Applied Sciences. We would also like to thank the observers and lecturers from OPTIMAX 2017, as well as Dr. Annemieke Meijer, Professor Peter Hogg and Associate Professor Asbjørn Johannessen for their contributions.

References

1. Miller DL, Rehani MM. Overview of ICRP Committee 3 " Protection in Medicine." ICRP 2013 Proc. 2013;(121):24–32.
2. Berger RP, Panigrahy A, Gottschalk S, Sheetz M. Effective Radiation Dose in a Skeletal Survey Performed for Suspected Child Abuse. *J Pediatr*. Elsevier Inc.; 2016;171:310–2.
3. Hoffman DA, Lonstein JE, Morin MM, Hi BSHH, Boice JD. Breast Cancer in Women with Scoliosis Exposed to multiple diagnostic x-rays. *JDCI Oxford J*. 2005;81(17):1–6.
4. Phillips KL, Bastin ST, Davies-payne D, Browne D, Bird HL, Craw S, et al. Radiographic skeletal survey for non-accidental injury : Systematic review and development of a national New Zealand protocol. 2015;59:54–65.
5. Pablot SM. 1996, *The British Journal of Radiology*, 69, 437–450. 1996;69(821):437–50.
6. Jones A, Ansell C, Jerrom C, Honey ID. Optimization of image quality and patient dose in radiographs of paediatric extremities using direct digital radiography. *Br J Radiol* [Internet]. The British Institute of Radiology; 2015 Mar 27;88(1050):20140660. Available from: <https://doi.org/10.1259/bjr.20140660>
7. Busch HP. Need for New Optimisation Strategies in CR and Direct Digital Radiography. *Radiat Prot Dosimetry*. 2000;90(1):31–3.
8. Mooney R, Thomas PS. Dose reduction in a paediatric X-ray department following optimization of radiographic technique. *Br J Radiol*. 1998;71(AUG.):852–60.
9. Brosi P, Stuessi A, Verdun FR, Vock P, Wolf R. Copper filtration in pediatric digital X-ray imaging: Its impact on image quality and dose. *Radiol Phys Technol*. 2011;4(2):148–55.
10. Goske MJ, Charkot E, Herrmann T, John SD, Mills TT, Morrison G, et al. Image Gently: challenges for radiologic technologists when performing digital radiography in children. *Pediatr Radiol* [Internet]. 2011 May [cited 2012 Mar 13];41(5):611–9. Available from: <http://www.ncbi.nlm.nih.gov/pubmed/21491201>
11. Strauss KJ, Frush DP, Goske MJ. Invited Paper Image Gently Campaign : Making a World of Difference. *Med Phys Int J*. 2015;3(2):94–108.
12. Clement C, Sasaki M, Khong P-L, Ringertz V, Donoghue D, Frush M, et al. ICRP, 2013. Radiological Protection in Paediatric Diagnostic and Interventional Radiology. *Compend Dose Coefficients based ICRP Publ 60*. 2012;42(2):130.
13. Whole P, Phantom B. Pediatric Whole Body Phantom " PBU-70 ". Kyoto Kagaku. :2.
14. Catalog PP-70. Lungs Pulmonary Vessels Mediastinum Liver Kidneys. *Pediatr Whole body Phantom*. :2.
15. Slovis TL, Strouse PJ, Strauss KJ. Radiation Exposure in Imaging of Suspected Child Abuse: Benefits versus Risks. *J Pediatr*. Elsevier Inc; 2015;167(5):963–8.
16. Canon. DelftDI Modality Overview. Canon, Canon Groep. :13.
17. CanonDetetor-Wireless C. Upgrade to DR in less than 2 minutes with just 2 components CXDI-701C Wireless Breath new life into your existing equipment ; fixed, mobile, even portable benefit from DR instantly. Canon. :4.
18. Canon-Intuition TD. DelftDI Intuition DR The DelftDI Intuition. Canon. :2.
19. Fritz S, Jones AK. Guidelines for anti-scatter grid use in pediatric digital radiography. *Pediatr Radiol*. 2014;44(3):313–21.
20. Knight SP. A paediatric X-ray exposure chart. *J Med Radiat Sci*. 2014;61(3):191–201.
21. Toivonen M. Patient dosimetry protocols in digital and interventional radiology. *Radiat Prot Dosim*. 2001;94(1–2):105–8.
22. Burger W, Burge M. Digital Image Processing: An Algorithmic Introduction Using Javae. 2008. p. 2.
23. Mori M, Imai K, Ikeda M, Iida Y, Ito F, Yoneda K, et al. Method of measuring contrast-to-noise ratio (CNR) in nonuniform image area in digital radiography. *Electron Commun Japan*. 2013;96(7):32–41.
24. Svensson S, Zachrisson S, Svalkvist A, Ba M, Ha M, Radiology D, et al. View Dex : an Efficient and Easy-To-Use Softw Are. *Radiat Prot Dosimetry*. 2010;139(1):42–51.
25. Park CM, Lee HJ, Goo JM, Han DH, Kim JH, Lim KY, et al. Comparison of observer performance on soft-copy reading of digital chest radiographs: High resolution liquid-crystal display monitors versus cathode-ray tube monitors. *Eur J Radiol*. 2008;66(1):13–8.

- 
26. Brennan PC, McEntee M, Evanoff M, Phillips P, O'Connor WT, Manning DJ. Ambient lighting: effect of illumination on soft-copy viewing of radiographs of the wrist. *AJR Am J Roentgenol.* 2007;188(2):177–80.
 27. Tashiro T, Manager G. 510 (k) summary; Monochrome LCD monitor MS25i2 (ML21025. 2013;10:8.
 28. McGinty, G, Allen B, Wald C. Imaging 3.0 ACR IT Reference Guide for the Practicing Radiologist. *Am Coll Radiol.* 2013;1–11.
 29. Mansson LG. Methods for the Evaluation of Image Quality: A Review. *Radiat Prot Dosimetry.* 2000;90(1):89–99.
 30. Lanca, Luis; Silva A. *Digital Imaging Systems for Plain Radiography.* Lisbon: Springer; 2013. 173 p.
 31. Mukaka MM. A guide to appropriate use of Correlation coefficient in medical research. *Malawi Med J.* 2012;24(3):69–71.
 32. Rennie L, Court-Brown CM, Mok JYQ, Beattie TF. The epidemiology of fractures in children. *Injury.* 2007;38(8):913–22.